

# Pt<sup>II</sup>-Catalyzed Hydrophenylation of $\alpha$ -Olefins: Variation of Linear/Branched Products as a Function of Ligand Donor Ability

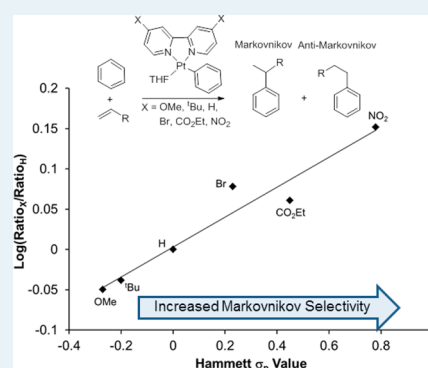
Bradley A. McKeown,<sup>†</sup> Bruce M. Prince,<sup>‡</sup> Zoraida Ramiro,<sup>†</sup> T. Brent Gunnoe,<sup>\*,†</sup> and Thomas R. Cundari<sup>\*,‡</sup>

<sup>†</sup>Department of Chemistry, University of Virginia, Charlottesville, Virginia 22904, United States

<sup>‡</sup>Center for Advanced Scientific Computing and Modeling (CASCaM), Department of Chemistry, University of North Texas, Denton, Texas 76203, United States

## S Supporting Information

**ABSTRACT:** The Pt<sup>II</sup> complexes [(<sup>x</sup>bpy)Pt(Ph)(THF)]<sup>+</sup> (<sup>x</sup>bpy = 4,4'-X<sub>2</sub>-2,2'-bipyridyl; x = OMe (1a), <sup>t</sup>Bu (1b), H (1c), Br (1d), CO<sub>2</sub>Et (1e) and NO<sub>2</sub> (1f)) catalyze the formation of *n*-propylbenzene and cumene from benzene and propene. The catalysts are selective for branched products, and the cumene/*n*-propylbenzene ratio decreases with increasing donor ability of the <sup>x</sup>bpy ligand. DFT(D) calculations predict more favorable activation barriers for 1,2-insertion into the Pt–Ph bond to give branched products. The calculations indicate that 1,2-insertion of propene should be faster than 2,1-insertion for all Pt(II) catalysts studied, but they also indicate that cumene/*n*-propylbenzene selectivity is under Curtin–Hammett control.

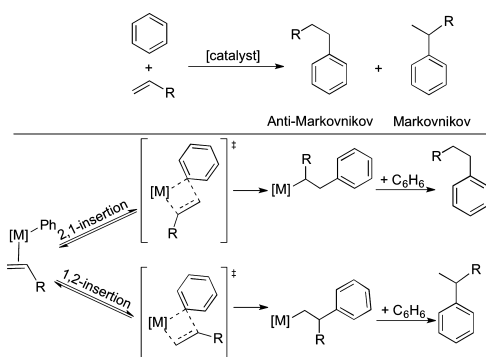


**KEYWORDS:** platinum, hydroarylation,  $\alpha$ -olefins, C–H activation, Curtin–Hammett principle

## INTRODUCTION

Transition-metal-catalyzed hydroarylation of substituted olefins by a nonacidic pathway (i.e., non-Friedel–Crafts catalysis) offers the opportunity to control the regioselectivity of olefin insertion into the M–aryl bond to obtain either Markovnikov or anti-Markovnikov products.<sup>1</sup> For example, catalysts that can bias 2,1- over 1,2-insertion with  $\alpha$ -olefins could selectively produce linear alkyl arenes that are not accessible with acid-based methodologies (Scheme 1).<sup>2</sup> The hydrophenylation of  $\alpha$ -olefins using Ru or Ir catalyst precursors has been reported to

**Scheme 1. Product Selectivity from Transition Metal Mediated Hydrophenylation of  $\alpha$ -Olefins Can Be Dictated by the Selectivity of Insertion into the M–Ph Bond**



favor the formation of the anti-Markovnikov over Markovnikov addition products with moderate selectivity ( $\sim$ 1.5:1 linear-to-branched ratio for both catalysts).<sup>1a,3</sup>

Unlike the Ir and Ru catalysts, product selectivity for Pt<sup>II</sup>-catalyzed hydrophenylation of propylene favors Markovnikov addition products. Goldberg and co-workers reported that a (pyridyl)pyrrolide ligated Pt<sup>II</sup> catalyst precursor catalyzes the formation of cumene and *n*-propylbenzene from benzene and propylene in an  $\sim$ 6:1 ratio.<sup>4</sup> In addition, we have reported that [(<sup>t</sup>bpy)Pt(Ph)(THF)][BAr'<sub>4</sub>] (1b; <sup>t</sup>bpy = 4,4'-di-*tert*-butyl-2,2'-bipyridine; Ar' = 3, 5-(CF<sub>3</sub>)<sub>2</sub>-C<sub>6</sub>H<sub>3</sub>) catalyzes the formation of cumene and *n*-propylbenzene in an  $\sim$ 3:1 ratio (Chart 1).<sup>5</sup> Vitagliano and Tesaro studied the stoichiometric C–C bond formation from cationic Pt<sup>II</sup>(aryl)(olefin) (aryl = C<sub>6</sub>H<sub>5</sub>, 4-C<sub>6</sub>H<sub>4</sub>R, or 3-C<sub>6</sub>H<sub>4</sub>R; R = OMe or Me) complexes containing *N,N* bidentate ligands.<sup>6</sup> These complexes effectively mediate migratory insertion of H<sub>2</sub>C=CHR (R = H, Me, or Ph) into the Pt–C<sub>aryl</sub> bond. Consistent with the results from Pt<sup>II</sup>-catalyzed propene hydrophenylation, 1,2-insertion and subsequent protonolysis yields the branched product.

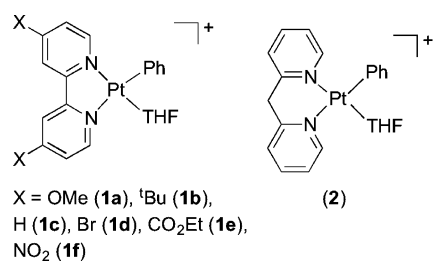
The proposed mechanism for transition-metal-catalyzed olefin hydrophenylation involves two principal steps: olefin insertion into the M–Ph bond and benzene C–H activation (Scheme 2).<sup>1,3,4,7</sup> The Pt<sup>II</sup> complex 1b has been demonstrated

Received: October 29, 2013

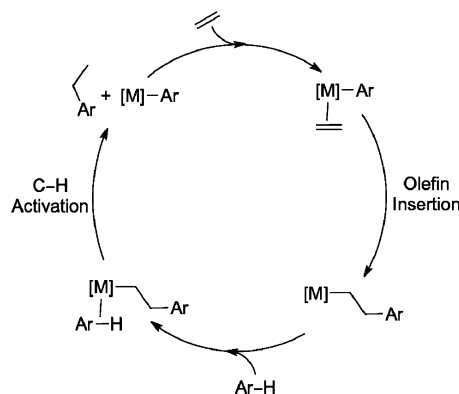
Revised: April 7, 2014

Published: April 22, 2014

Chart 1. Catalysts Studied for Hydroarylation of Substituted Olefins



Scheme 2. Generic Catalytic Cycle for Transition-Metal-Catalyzed Olefin Hydroarylation Proposed for Ru-, Ir- and Pt-based Catalyst Precursors



to insert ethylene into the Pt–Ph bond in the presence of excess olefin to yield  $[(^t\text{bpy})\text{Pt}(\text{CH}_2\text{CH}_2\text{Ph})(\eta^2\text{-C}_2\text{H}_4)]^+$ , which is the proposed resting state of catalytic ethylene hydrophenylation.<sup>7h,8</sup> We recently reported that expansion of the chelate ring size using  $[(\text{dpm})\text{Pt}(\text{Ph})(\text{THF})][\text{BAR}'_4]$  (**2**; dpm = di(2-pyridyl)methane) results in an increase in the catalytic efficiency for ethylene hydrophenylation.<sup>8a</sup>

As previously reported,<sup>8b</sup> the donor ability of bipyridyl ligands for Pt<sup>II</sup> catalyzed ethylene hydrophenylation influences the selectivity for ethylbenzene vs styrene, and we sought to determine the extent to which ancillary ligand donor ability could be used to alter selectivity for hydrophenylation of  $\alpha$ -olefins. In this report, catalytic activity is evaluated using longer-chain and internal olefins as well as Michael acceptors for complexes **1b** and **2**. The impact of 2,2'-bipyridyl ligand donor ability on Pt<sup>II</sup>-catalyzed hydroarylation of  $\alpha$ -olefins is examined using various 2,2'-bipyridyl ligands with different 4,4' substituents (Chart 1). A clear trend for the influence of bpy donor ability has been established.

## RESULTS AND DISCUSSION

The hydroarylation of substituted olefins was studied using complexes **1b** and **2** as catalyst precursors. Under conditions of 0.01 mol % catalyst relative to benzene (1 mM Pt and 11 M benzene) and 0.1 MPa of propylene at 100 °C, catalysis with complex **1b** results in 33.5 (4 h) and 39.8 (16 h) turnovers (TO) of cumene and *n*-propylbenzene in an approximate 3:1 ratio (Table 1). Traces of isomers of di- and tripropylbenzenes were also detected. Although the formation of the Markovnikov addition product cumene is favored, the observation of significant quantities of the anti-Markovnikov addition product *n*-propylbenzene (~10 TO after 16 h) provides further support

Table 1. Hydrophenylation of Olefins with  $[(^t\text{bpy})\text{Pt}(\text{Ph})(\text{THF})][\text{BAR}'_4]$  (**1b**).<sup>a</sup>

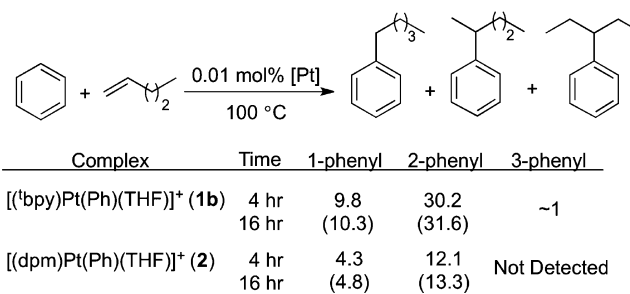
Olefin	Alkyl benzene	B:L <sup>b</sup>
	 25.0 <sup>e</sup> (29.7) <sup>f</sup>	 8.5 (10.1)
	 30.2 (31.6)	 9.8 (10.3)
	 18.9 (20.9)	–

<sup>a</sup>0.01 mol % catalyst (1 mM) dissolved in C<sub>6</sub>H<sub>6</sub> with hexamethylbenzene as an internal standard at 100 °C. <sup>b</sup>Ratio of branched to linear isomer after 4 h. <sup>c</sup>0.1 MPa C<sub>3</sub>H<sub>6</sub>; see ref 10. <sup>d</sup>150 equiv relative to Pt. <sup>e</sup>Turnovers after 4 h as determined by GC/MS. <sup>f</sup>Numbers in parentheses are turnovers after 16 h.

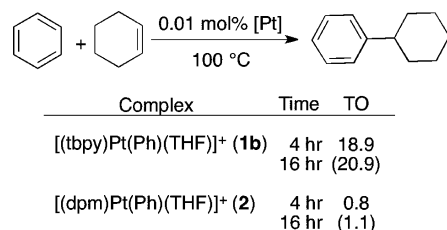
for a nonacid-catalyzed mechanism because acid-based catalysts are highly selective for Markovnikov addition.<sup>2</sup>

Increasing the length of the carbon chain upon substitution of 1-pentene for propylene has a minimal influence on catalyst efficiency and selectivity. Using 150 equiv of 1-pentene (relative to **1b**), 40 TO of 2-phenylpentane and *n*-pentylbenzene were observed after 4 h at 100 °C in a ~3:1 ratio with no further activity observed after this time point. The formation of approximately 1 equiv (relative to catalyst) of 3-phenylpentane during the hydrophenylation of 1-pentene using complex **1b** indicates that olefin isomerization occurs but is not significantly competitive on the time scale of catalysis. The catalyst is also compatible with disubstituted olefins, as the reaction with cyclohexene results in ~20 TO of phenylcyclohexane after 16 h at 100 °C.

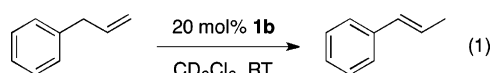
The efficiency of catalytic hydrophenylation of substituted olefins using complex **2** is reduced compared to complex **1b**.<sup>9</sup> Using **2**, propylene hydrophenylation results in 11.8 TO of cumene and *n*-propylbenzene after 4 h in a 4.4:1.0 ratio. Catalysis with 1-pentene and cyclohexene using **2** also results in a reduction in TO compared to the 2,2'-bipyridyl complex **1b** (Schemes 3 and 4). Although **2** is a more effective catalyst for ethylene hydrophenylation,<sup>8a</sup> its efficacy for hydrophenylation of  $\alpha$ -olefins is reduced relative to **1b**. We believe that the reduced activity of **2** relative to **1b** is a result of the increased steric bulk of the dpm ligand compared to <sup>t</sup>bpy.

Scheme 3. Comparison of Catalytic Hydrophenylation of 1-Pentene (150 equiv relative to Pt) Using Complexes **1b** and **2** (0.01 mol % relative to benzene)

**Scheme 4. Comparison of Catalytic Hydrophenylation of Cyclohexene (150 equiv relative to Pt) Using Complexes 1b and 2 (0.01 mol %, 1 mM, relative to benzene)**



Intramolecular olefin hydroarylation was attempted with allylbenzene to form indane (eq 1). Heating complex **1b** or **2** in



neat allylbenzene at 100 °C resulted in trace amounts of indane (observed by GC/MS). The small amount of cyclized product is not surprising because successful catalysis requires activation of an ortho C–H bond of allylbenzene, and product distributions from ethylene hydroarylation using substituted benzenes demonstrate that ortho C–H activation is not favored relative to meta or para activation.<sup>7h</sup> In addition, cationic Pt<sup>II</sup> complexes containing phenyl ligands have been reported to be active for the isomerization of allylbenzene to the internal olefin *trans*- $\beta$ -methyl-styrene.<sup>10</sup> Analysis of the mixture from reaction of both the <sup>t</sup>bpy complex **1b** and the dpm complex **2** with allylbenzene reveals that both of these Pt complexes catalyze olefin isomerization. Monitoring the reaction of **1b** (20 mol % relative to substrate) and allylbenzene in CD<sub>2</sub>Cl<sub>2</sub> by <sup>1</sup>H NMR spectroscopy shows complete conversion of allylbenzene to *trans*- $\beta$ -methyl-styrene in ~1 h at room temperature (eq 1).

**Functionalized Olefins.** Hydrophenylation of  $\alpha,\beta$ -unsaturated carbonyl compounds by complex **1b** was performed to probe catalyst tolerance toward heteroatomic functionality (Table 2). In all cases, catalysis was selective for the anticipated Michael addition product. Catalysis in benzene for 4 h with 0.01 mol % **1b** and 150 equiv of methacrylate (relative to **1b**) at 100 °C results in the formation of 6.8 TO of methyl 3-

**Table 2. Hydrophenylation of Michael Acceptors Using [(<sup>t</sup>bpy)Pt(Ph)(THF)][BAR'<sub>4</sub>] (**1b**)<sup>a</sup>**

Olefin	Addition Product	TO	TO
		6.8 <sup>b</sup> (6.9) <sup>c</sup>	4.9 (5.2)
		~7 <sup>d</sup> (~7) <sup>d</sup>	Trace
		0.7 (1.3)	Trace
		1.6 (1.9)	

<sup>a</sup>0.01 mol % catalyst (1 mM) dissolved in C<sub>6</sub>H<sub>6</sub> with 150 equiv of olefin (relative to Pt loading) and hexamethylbenzene as an internal standard at 100 °C. <sup>b</sup>Turnovers after 4 h as determined by GC/MS. <sup>c</sup>Numbers in parentheses are turnovers after 16 h. <sup>d</sup>Turnovers estimated from GC peak area ratios between product and internal standard. <sup>e</sup>Catalysis performed at 120 °C.

phenylpropanoate and 4.9 TO of methyl cinnamate (11.7 total TO). This corresponds to a 1.4:1 ratio of saturated to unsaturated products. No further catalytic activity was observed with continued reaction.

The same reaction was performed using methyl methacrylate to determine if the presence of an  $\alpha$ -methyl group would inhibit  $\beta$ -hydride elimination after insertion into the Pt–Ph bond and increase selectivity for the saturated addition product. Indeed, the dominant product from catalysis was 2-methyl-3-phenylpropanoate, which was identified by GC/MS and comparison after catalysis of the <sup>1</sup>H NMR spectrum of the reaction mixture to reported NMR data.<sup>11</sup> Only trace amounts of 2-methyl-3-phenyl-2-propenoate were observed. Because of a lack of analytically pure material, linear regressions for quantification were not performed, but using the ratio of product to internal standard peak areas, ~7 TO of 2-methyl-3-phenylpropanoate is estimated from catalysis with **1b** and methyl methacrylate in benzene. Catalysis with methyl vinyl ketone (MVK) or cyclohexenone is less efficient than the analogous reactions with the ester derivatives. For MVK, increased temperature (120 °C) was required to observe the addition product 4-phenylbutan-2-one, but only in near stoichiometric amounts. Approximately 2 TO of 3-phenylcyclohexanone is observed after 16 h at 100 °C for the hydrophenylation of cyclohexenone.

**Use of 4,4'-Substituted Bipyridyl Ligands.** The series of complexes [(<sup>x</sup>bpy)Pt(Ph)(THF)][BAR'<sub>4</sub>] [<sup>x</sup>bpy = 4,4'-X<sub>2</sub>-2,2'-bipyridyl; X = OMe (**1a**), <sup>t</sup>Bu (**1b**), H (**1c**), Br (**1d**), CO<sub>2</sub>Et (**1e**), and NO<sub>2</sub> (**1f**)] was screened for propylene hydrophenylation to evaluate the influence of ligand donor ability on product selectivity (Table 3). Catalysis with complexes **1a**–**1c** demonstrates a slight enhancement in catalytic efficiency compared with catalysis with **1d**–**1f**, which is the same trend in catalyst efficiency that has been observed for ethylene hydrophenylation.<sup>8b</sup> Catalyst precursors **1d**–**1f** exhibit a greater predilection for the formation of unsaturated products (i.e.,

**Table 3. Comparison of Catalytic Propylene Hydrophenylation Using Complexes 1a–1f.<sup>a</sup>**

X	$\sigma_p$	<sup>1</sup> Pr	<sup>n</sup> Pr	B:L <sup>b</sup>
OMe ( <b>1a</b> )	-0.27	10.6 <sup>c</sup> (26.9) <sup>d</sup>	3.7 (9.7)	2.9
<sup>t</sup> Bu ( <b>1b</b> )	-0.2	25.0 (29.7)	8.5 (10.1)	2.9
H ( <b>1c</b> )	0.0	25.8 (31.6)	8.0 (10.3)	3.2
Br ( <b>1d</b> )	0.23	2.5 (4.2)	0.7 (1.4)	3.8
CO <sub>2</sub> Et ( <b>1e</b> )	0.45	12.1 (18.3)	3.3 (5.1)	3.7
NO <sub>2</sub> ( <b>1f</b> )	0.78	4.1 (6.5)	0.9 (1.6)	4.6

<sup>a</sup>0.01 mol % catalyst dissolved in C<sub>6</sub>H<sub>6</sub> with hexamethylbenzene as an internal standard at 100 °C with 0.1 MPa C<sub>3</sub>H<sub>6</sub>. <sup>b</sup>Ratio of cumene to *n*-propylbenzene after 4 h. <sup>c</sup>Turnovers after 4 h as determined by GC/MS. <sup>d</sup>Numbers in parentheses are turnovers after 16 h.

isomers of (propenyl)benzene), as observed by GC/MS, relative to **1a**–**1c**. After 16 h at 100 °C, the nitro-substituted complex **1f** gives 8.1 TO of propylbenzenes with a 4.6:1.0 branched/linear ratio. In contrast, ethylene hydrophenylation using **1f** gives an approximately stoichiometric yield of ethylbenzene and styrene.<sup>8b</sup> The 1,2-insertion of propylene into the Pt–Ph bond forms the intermediate  $[(\text{NO}_2\text{-bpy})\text{Pt}(\text{CH}_2\text{CH}(\text{Me})\text{Ph})]^+$ , and the presence of the  $\beta$ -methyl group may result in a difference in activation barrier for  $\beta$ -hydride elimination relative to elimination of styrene from  $[(\text{NO}_2\text{-bpy})\text{Pt}(\text{CH}_2\text{CH}_2\text{Ph})]^+$ .<sup>12</sup>

The ratio of cumene/*n*-propylbenzene is influenced by the donor ability of the bipyridyl ligand. For example, catalysis using complex **1a** (OMe,  $\sigma_p = -0.27$ ) and 0.1 MPa of propylene (100 °C) results in a cumene/*n*-propylbenzene ratio of 2.9 (after 4 h) compared with 4.6 for complex **1f** ( $\text{NO}_2$ ,  $\sigma_p = 0.78$ ). A Hammett plot was constructed using product ratios (*n*-propylbenzene vs cumene), and the Hammett parameter,  $\sigma_p$  (Figure 1). Although the effects of substituted pyridyl ligands

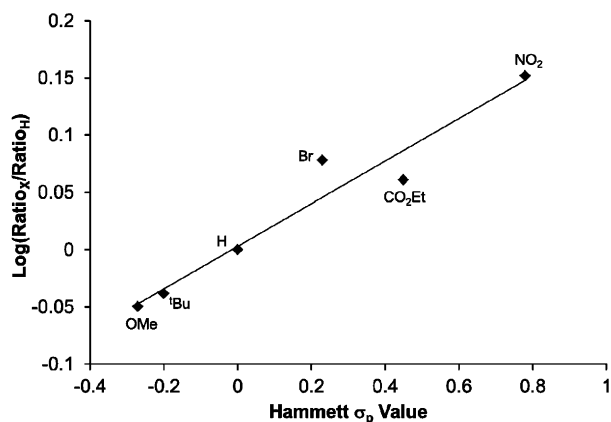
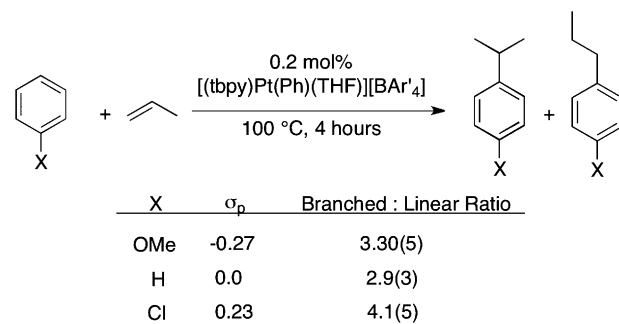


**Figure 1.** Hammett plot using the ratios of cumene to *n*-propylbenzene from  $[(^x\text{bpy})\text{Pt}(\text{Ph})(\text{THF})]^+$ -catalyzed propylene hydrophenylation after 4 h at 100 °C with 0.1 MPa of ethylene (slope = 0.2,  $R^2 = 0.94$ ).

are rarely amenable to Hammett correlations,<sup>13</sup> a good linear correlation is observed ( $R^2 = 0.94$ ). The plot demonstrates that less-donating 4,4' substituents result in an increase in the ratio of cumene/*n*-propylbenzene, but the magnitude of the slope ( $\rho = 0.2$ ) suggests that the ligand donor ability has a small, but clear and quantifiable, influence on the selectivity for propylene insertion into the Pt–Ph bond and overall product selectivity.

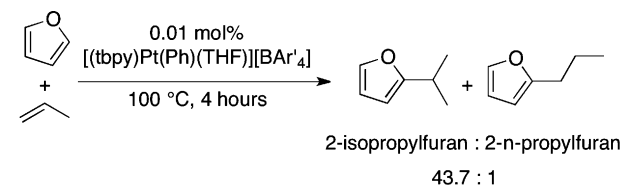
**Functionalized Arenes.** Next, we sought to determine the electronic effect of arene functionality on linear/branched selectivity. The isomers of propylene hydroarylation using anisole, benzene, and chlorobenzene were resolved using GC/MS. Only para-substituted isomers were used for comparison, but meta- and ortho-substituted benzenes were also observed. Comparing the peak area ratios of 4-<sup>x</sup>Pr-1-X-C<sub>6</sub>H<sub>4</sub> and 4-<sup>n</sup>Pr-1-X-C<sub>6</sub>H<sub>4</sub> (X = OMe, H and Cl) after 4 h of heating at 100 °C under 0.1 MPa of propylene with 0.2 mol % **1b** demonstrates no correlation between the Hammett  $\sigma_p$  parameter of the benzene functionality and Markovnikov/anti-Markovnikov product selectivity for the resulting alkyl arenes (Scheme 5). Catalysis with both anisole (OMe,  $\sigma_p = -0.27$ ) and chlorobenzene (Cl,  $\sigma_p = 0.23$ ) provides a greater predilection for formation of the isopropyl functionalized arene compared with that of benzene.

### Scheme 5. Comparison of Branched to Linear Ratios of Propylene (0.1 MPa) Hydroarylation Using Substituted Benzenes



Functional groups on benzene exert little influence on selectivity for catalytic propylene hydroarylation; however, the substitution of benzene for furan biases the reaction to favor the Markovnikov addition product by a substantial amount (Scheme 6). After 4 h at 100 °C, complex **1b** catalyzes the

### Scheme 6. Ratio of 2-Isopropylfuran and 2-*n*-Propylfuran from Propylene (0.1 MPa) Hydroarylation with Furan and $[(^x\text{bpy})\text{Pt}(\text{Ph})(\text{THF})]^+$ at 100 °C after 4 h, as Determined from Peak Area Ratios from Analysis by GC/MS



formation of 2-isopropylfuran and 2-*n*-propylfuran in an approximate 44:1 ratio, as determined by comparison of peak areas from GC/MS analysis.

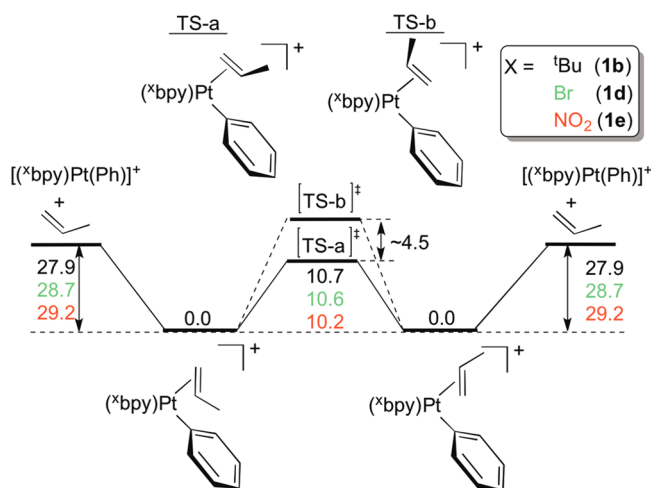
**Computational Studies.** Density functional theory (DFT-(D)) was employed to probe hydroarylation of  $\alpha$ -olefins catalyzed by  $[(^x\text{bpy})\text{Pt}(\text{Ph})]^+$  complexes ( $x = \text{tBu}, \text{NO}_2$  or Br). The Gaussian 09<sup>14</sup> package was used to perform all simulations. All stationary points were obtained using the B3LYP<sup>15</sup> functional with a pseudopotential scheme that is valence double- $\zeta$ -plus-polarization (CEP-31G(d)) on the main group elements and triple- $\zeta$  on the transition metals. Reported Gibbs free energies were determined at 298.15 K and 1 atm and utilize unscaled B3LYP/CEP-31G(d)<sup>16</sup> vibrational frequencies. The D3(BJ) dispersion correction<sup>17</sup> with Becke–Johnson damping<sup>18</sup> was utilized. The modeled system is cationic; thus, the CPCM<sup>19</sup> formalism was used with THF ( $\epsilon = 7.43$ ) as the solvent. Stationary points were differentiated as minima or transition states (TSs) via computation of the energy Hessian and observation of the correct number of imaginary frequencies, zero (0) and one (1), respectively. Intrinsic reaction coordinates<sup>20</sup> from the TS geometries were computed. All geometry optimizations were performed without symmetry or coordinate restraint, and all complexes were singlets for which restricted Kohn–Sham theory<sup>21</sup> was employed.

Product selectivity for the hydrophenylation of propylene (i.e., linear/branched ratios) could be determined by the regioselectivity of olefin insertion or by the relative rates of subsequent reactions (i.e., Curtin–Hammett conditions). Provided that olefin insertion into the Pt–Ph bond is reversible,

as depicted in Scheme 1, the formation of cumene could be preferential because of more favorable barriers for benzene coordination or C–H activation. Thus, we calculated the energetics of all steps, starting from propylene coordination to the Pt<sup>II</sup> complexes. For the computational modeling, we focused on three Pt complexes: [(<sup>t</sup>bpy)Pt(Ph)]<sup>+</sup> (**1b**), [(<sup>Br</sup>bpy)Pt(Ph)]<sup>+</sup> (**1d**), and [(<sup>NO<sub>2</sub></sup>bpy)Pt(Ph)]<sup>+</sup> (**1f**).

The energetics of the coordinated propylene complexes [(<sup>x</sup>bpy)Pt(Ph)( $\eta^3$ -C<sub>3</sub>H<sub>6</sub>)]<sup>+</sup> were studied to assess the preferred olefin binding mode. Calculated stationary points relevant to propylene binding are depicted in Scheme 7 for  $x = {}^t\text{Bu}$  (black),

**Scheme 7.** B3LYP-D3(BJ)/CEP-31G(d)/THF-Calculated Propylene Binding and Rotational Transition States for [(<sup>x</sup>bpy)Pt(Ph)( $\eta^2$ -C<sub>3</sub>H<sub>6</sub>)]<sup>+</sup><sup>a</sup>



<sup>a</sup>The Gibbs free energy values are given in kcal/mol. The 2,2'-bipyridyl ligand with 4,4'-substituents are color coded:  $x = {}^t\text{Bu}$  (black), Br (green), NO<sub>2</sub> (red). Propylene adduct isomers are differentiated by whether the propylene methyl group is proximal or distal to the phenyl ligand, but are nearly degenerate. Model propylene rotational transition states feature the propylene methyl group proximal (TS-a, left) or distal (TS-b, right) to the phenyl ligand.

Br (green), and NO<sub>2</sub> (red) supporting ligand models. In the ground state of [(<sup>x</sup>bpy)Pt(Ph)( $\eta^2$ -C<sub>3</sub>H<sub>6</sub>)]<sup>+</sup>, the C=C bond of propylene is perpendicular to the platinum square plane, which is common for square planar d<sup>8</sup> transition metals.<sup>7h,8a,22</sup> Isomers of propylene coordination are thus differentiated by whether the propylene methyl group is proximal or distal to the phenyl ligand. There is, however, negligible calculated free energy difference (<0.1 kcal/mol) between these isomers for [(<sup>x</sup>bpy)Pt(Ph)( $\eta^2$ -C<sub>3</sub>H<sub>6</sub>)]<sup>+</sup>, implying minimal steric contact between the propylene methyl moiety and the remainder of the complex. Computations revealed subtle distinctions in the propylene rotational barriers and more so in the propylene binding free energies, which are linked to the electronic properties of the bipyridyl substituents (Scheme 7).

Rotation of propylene about the metal/C=C centroid axis leads to two isomeric rotational transition states (Scheme 7 and Figure 2) in which the methyl group of the propylene is either proximal (TS-a) or distal (TS-b) to the phenyl ring, respectively. In the rotational transition states, the C=C bond is in the square plane of the Pt complex. For all complexes modeled, TS-a in Scheme 7 was computed to be lower by ~4 kcal/mol than TS-b, presumably because of steric hindrance between the methyl group on propylene and a 6-H

on the bipyridyl ligand. For all three catalyst models, the calculated  $\Delta G_{\text{rot}}^\ddagger$  is ~10–11 kcal/mol. There is good agreement between experiment and theory for olefin rotation. For [(<sup>t</sup>bpy)Pt(CH<sub>2</sub>CH<sub>2</sub>Ph)( $\eta^2$ -C<sub>2</sub>H<sub>4</sub>)]<sup>+</sup>, the experimentally determined  $\Delta G_{\text{rot}}^\ddagger$  for ethylene rotation is 11.7 kcal/mol at –33.4 °C, and the calculated  $\Delta G_{\text{rot}}^\ddagger$  is 12.4 kcal/mol.<sup>7h</sup> For all three modeled complexes, the dissociation of propylene from [(<sup>x</sup>bpy)Pt(Ph)( $\eta^2$ -C<sub>3</sub>H<sub>6</sub>)]<sup>+</sup> is calculated to be endergonic by >27 kcal/mol, which is higher by at least 17 kcal/mol in comparison to the propylene rotational transition states (Scheme 7). This suggests that interconversion of the two propylene adduct conformers will involve rotation of the olefin rather than dissociation and recoordination of propylene. When  $x = \text{NO}_2$  or Br, propylene binding to the Pt complex is calculated to be more exergonic by 1.3 or 0.8 kcal/mol, respectively, as compared with [(<sup>t</sup>bpy)Pt(Ph)]<sup>+</sup> (Scheme 7), which can likely be attributed to the electron-withdrawing nitro or bromo groups on the bpy, which enhances olefin coordination by providing a more electrophilic Pt center.

**Selectivity for Branched vs Linear Insertion.** Two isomeric pathways for propylene insertion into the Pt–phenyl bond were investigated from [(<sup>x</sup>bpy)Pt(Ph)( $\eta^2$ -C<sub>3</sub>H<sub>6</sub>)]<sup>+</sup>. The two products of propylene insertion yield cumene or *n*-propylbenzene after benzene C–H activation (Scheme 8). For the <sup>t</sup>bpy complex, computations reveal a  $\Delta\Delta G_{\text{ins}}^\ddagger = 1.6$  kcal/mol between transition states for propylene insertion with the lower energy transition state leading to the branched product (Scheme 8). At the same level of theory, relative free energy barriers ( $\Delta\Delta G_{\text{ins}}^\ddagger$ ) for propylene insertion into the (<sup>NO<sub>2</sub></sup>bpy)Pt–Ph and (<sup>Br</sup>bpy)Pt–Ph bonds were 2.0 and 1.6 kcal/mol. Similar to the <sup>t</sup>bpy complex, the  $\Delta G_{\text{ins}}^\ddagger$  leading to the branched product is lower than for the linear product in <sup>NO<sub>2</sub></sup>bpy and <sup>Br</sup>bpy cases. DFT(D) predicts a slightly enhanced kinetic selectivity for the branched product for the <sup>NO<sub>2</sub></sup>bpy complex relative to the <sup>t</sup>bpy complex, which is consistent with experimental branched/linear ratios from catalytic hydrophenylation of propylene (see Table 3 and Figure 1). However, as discussed below, the relative rates of 1,2- vs 2,1-propene insertion may not dictate the ultimate selectivity for formation of cumene vs *n*-propylbenzene.

Analysis of atomic charges for the olefin insertion TSs did not reveal any obvious trends to explain product selectivity for 1,2- vs 2,1-insertion as a function of the <sup>x</sup>bpy ligand, as expected, given the similar inductive impact of H and methyl substituents. Analysis of the geometries of the propylene insertion TSs showed very modest changes (typically <<0.05 Å) in bond lengths as a function of the X group or the insertion regiochemistry. In addition, differences in computed electronic energies and enthalpies and free energies were nearly identical, suggesting that preference for insertion mode is due to the looseness or tightness of the TS is not at the root of the observed and computed selectivity differences. The calculations reveal that the 1,2-insertion products are more stable than the 2,1-insertion products by 1.6 (<sup>t</sup>bpy), 1.5 (<sup>Br</sup>bpy), and 1.5 kcal/mol (<sup>NO<sub>2</sub></sup>bpy).

**Catalytic Cycle.** The catalytic cycle for hydrophenylation was investigated using DFT(D). For the <sup>t</sup>bpy catalyst, the potential energy surface (PES) depicts the energy pathway leading to branched and linear alkyl arene (Scheme 9). The reaction coordinates for other catalyst models are similar to Scheme 9 (see Supporting Information). The pertinent free energies for all modeled catalysts are collected in Table 4.

There are two plausible mechanisms for arene C–H bond activation: oxidative hydrogen migration (OHM) and oxidative

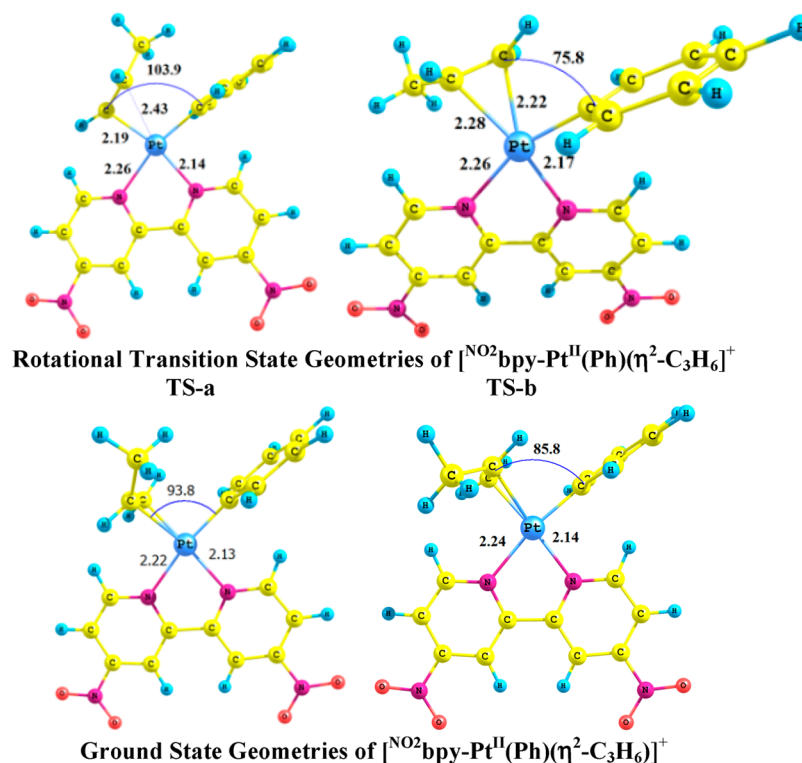
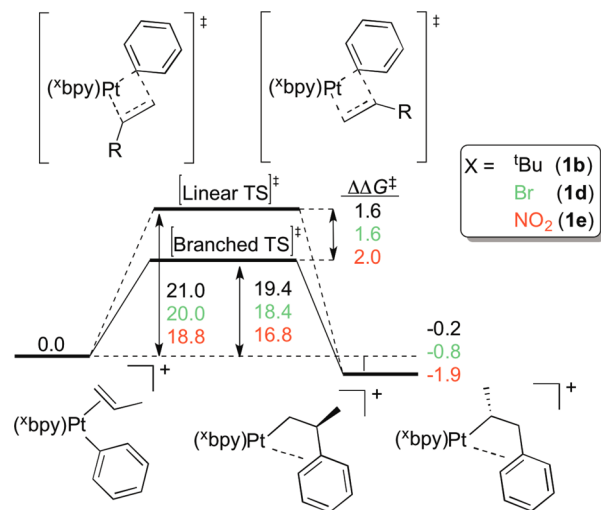


**Figure 2.** B3LYP/CEP-31G(d)/THF-calculated transition state geometries (top) for propylene rotation and ground state geometries (bottom) for the complex  $[(\text{NO}_2\text{bpy})\text{Pt}(\text{Ph})(\eta^2\text{-C}_3\text{H}_6)]^{\dagger}$ . Bond lengths are in angstroms, and angles are in degrees. Related  ${}^t\text{bpy}$  and  ${}^{\text{Br}}\text{bpy}$  geometries are in the Supporting Information. Note that geometries differ in the orientation of the methyl substituent on propylene relative to the remainder of the catalyst.

**Scheme 8. Calculated Free Energies (kcal/mol) for Propylene Insertion into the Pt–Ph Bond Starting from  $[(^{\text{X}}\text{bpy})\text{Pt}(\text{Ph})(\eta^2\text{-C}_3\text{H}_6)]^{\dagger}$**



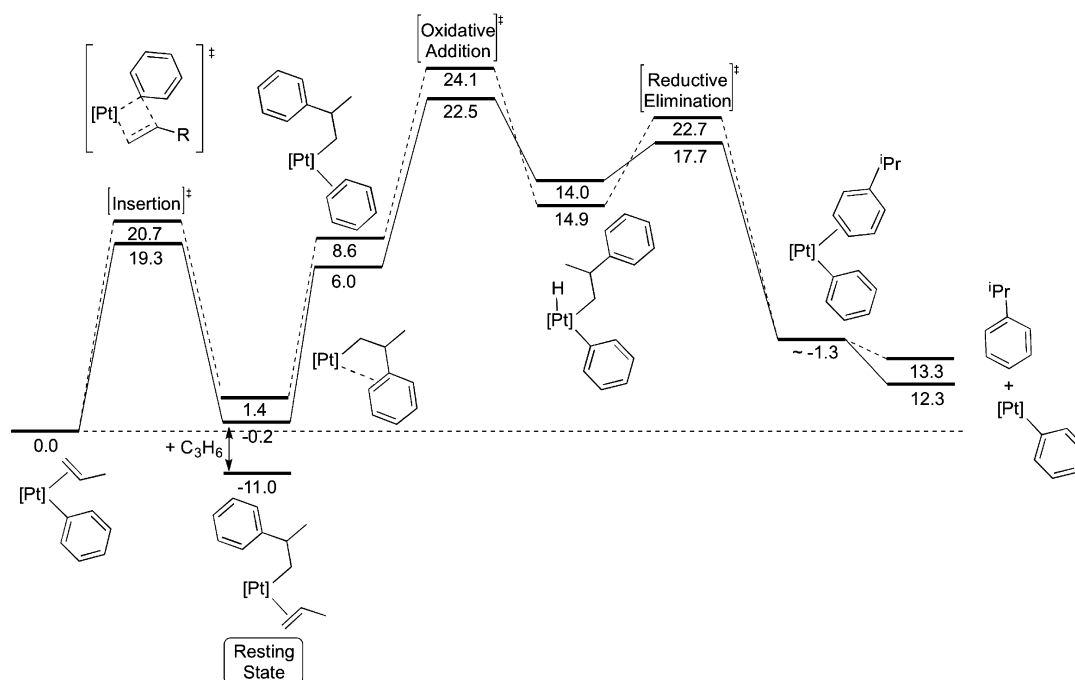
addition/reductive elimination (OA/RE), with the latter calculated to be the preferred pathway. A typical benzene oxidative addition TS, which defines the highest computed point on the PES, leading to a branched product, is shown in Figure 3; all other Cartesian coordinates are collected in the Supporting Information.

The benzene C–H activation barrier has been previously reported to be the rate-determining step for catalytic ethylene hydrophenylation catalyzed by **1b**.<sup>7h</sup> Relative to the most stable propylene adduct,  $[(^t\text{bpy})\text{Pt}(\text{Ph})(\eta^2\text{-propylene})]^{\dagger}$ , the calcu-

lated transition state leading to cumene is 22.5 kcal/mol. This is lower in free energy by 1.6 kcal/mol in comparison to the TS for pathway leading to *n*-propylbenzene (Scheme 9 and Table 4). For the  $\text{NO}_2\text{bpy}$  model, the lowest energy benzene C–H oxidative addition TS is 21.3 kcal/mol (Table 4), lower by 1.2 kcal/mol than for the  ${}^t\text{bpy}$  derivative, but nearly identical to the  ${}^{\text{Br}}\text{bpy}$  catalyst model. Hence, simulations suggest commensurate activity for the electron-withdrawing substituents, and each marginally lower than the  ${}^t\text{bpy}$  congener. In all cases, cumene is predicted to be the preferred product of hydrophenylation of propylene, as is observed experimentally.

Above, we used DFT(D) calculations to assess the kinetic selectivity for 1,2- vs 2,1-insertion, but the calculated energetics suggest that Curtin–Hammett conditions would apply to the  $\text{Pt}^{\text{II}}$  catalyzed propylene hydrophenylation. Thus, the rate of propylene deinsertion and reinsertion into the Pt–Ph bond is predicted to be faster than the rate of benzene C–H activation by either the 1,2- or 2,1-insertion product. Previously, we have reported that the resting state for catalytic hydrophenylation of ethylene using several Ru(II) or Pt(II) catalysts is the insertion product with coordinated ethylene,  $\text{M}(\text{CH}_2\text{CH}_2\text{Ph})(\eta^2\text{-ethylene})$ .<sup>1,21,23</sup> Although the spectra are complicated, monitoring the hydrophenylation of propene by **1b** using  ${}^1\text{H}$  NMR spectroscopy reveals resonances consistent with the analogous resting state. Table 4 shows calculated energetics for the production of cumene and *n*-propylbenzene for all three Pt complexes. Under Curtin–Hammett conditions, the predicted branched/linear ratio for each catalyst can be estimated using the relative activation barriers for rate-limiting benzene C–H activation. For the  ${}^t\text{bpy}$  complex, a  $\Delta\Delta G^{\ddagger}$  of 1.6 kcal/mol (favoring cumene production) would give a branched/linear

Scheme 9. Calculated Ground and Transition States for Propylene Hydrophenylation To Yield Cumene (solid line) or *n*-Propylbenzene (dashed line) Catalyzed by  $[(^t\text{bpy})\text{Pt}(\text{Ph})(\text{THF})][\text{BAR}'_4] (\mathbf{1b})^a$



<sup>a</sup>Similar pathways are calculated for the <sup>Br</sup>bpy ( $\mathbf{1d}$ ) and <sup>NO<sub>2</sub></sup>bpy ( $\mathbf{1f}$ ) derivatives; see Table 4. The Gibbs free energy barriers are in kcal/mol. Ground and transition state structures relevant to the formation of the preferred product, cumene, are shown.

Table 4. Relative Free Energies<sup>a</sup> for Olefin Hydroarylation with <sup>t</sup>bpyPt<sup>II</sup> Complex<sup>b</sup>

	<sup>t</sup> bpy cumene	<sup>t</sup> bpy <i>n</i> PB	<sup>NO<sub>2</sub></sup> bpy cumene	<sup>NO<sub>2</sub></sup> bpy <i>n</i> PB	<sup>Br</sup> bpy cumene	<sup>Br</sup> bpy <i>n</i> PB
$[(^t\text{bpy})\text{Pt}^{\text{II}}(\text{Ph})(\eta^3\text{-C}_3\text{H}_6)]^+$	0	0	0	0	0	0
insertion TS	19.3	20.7	16.5	18.4	18.3	19.7
benzene adduct	6.0	8.6	4.5	8.0	5.4	9.1
benzene OA TS	22.5	24.1	21.3	23.0	21.5	23.5
products	12.3	13.3	13.7	14.7	13.1	14.1

<sup>a</sup>(B3LYP/CEP-31G(d), STP, kcal/mol, in THF). <sup>b</sup>The superscript <sup>+</sup> denotes cationic complexes. All species are d<sup>8</sup> reactants and products with formally d<sup>6</sup>-hydride intermediates. OA = oxidative addition.

ratio of ~4:1 (at room temperature), which is similar to the experimental value of 2.9:1 at 100 °C. The same calculations for the <sup>NO<sub>2</sub></sup>bpy ( $\Delta\Delta G^\ddagger = 1.7$  kcal/mol) and the <sup>Br</sup>bpy ( $\Delta\Delta G^\ddagger = 2.0$  kcal/mol) predicts branched/linear ratios of 4.4:1 and 5.8:1, respectively. Although the calculations correctly predict that cumene is favored over *n*-propylbenzene for all ligands <sup>t</sup>bpy, the observed experimental trend for variation of branched/linear ratio is not reproduced. These results are not surprising, given the energy differences to accurately model the selectivity trend are much smaller than expected standard errors in the calculations. The most salient result from the calculations, which is well within expected errors, is that the branched/linear ratio is likely a function of Curtin–Hammett conditions and not controlled by the kinetic selectivity for 1,2- vs 2,1-insertion of propene into Pt–Ph bonds.

## CONCLUSIONS

In summary, cationic Pt<sup>II</sup> complexes supported by bipyridyl ligands are effective catalysts for the hydroarylation of

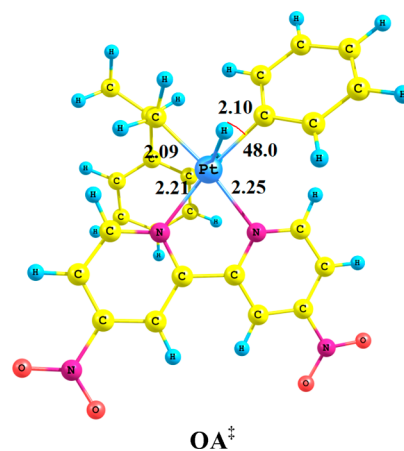


Figure 3. B3LYP/CEP-31G(d)/THF-calculated transition state geometry for C–H bond activation via oxidative addition by complex  $[(^{\text{NO}_2}\text{bpy})\text{Pt}(\text{CH}_2\text{CH}(\text{Ph})\text{CH}_3)]^+$ . Bond lengths are in angstroms, and angles are in degrees.

substituted olefins. The systematic variation of bipyridyl ligand electronic properties through 4,4'-substitution revealed a correlation between ligand donor ability and product selectivity for propylene hydrophenylation. Increasing the electron-withdrawing properties of the 4,4' substituent results in an increase in the cumene/*n*-propylbenzene ratio. Computational studies predict that 1,2-insertion (leading to branched product) is kinetically more favorable than 2,1-insertion of propene and that reducing the donor ability of the bpy ligands should further bias the insertion selectivity toward branched products. The results from the calculations also indicate that benzene C–H activation is rate-limiting for pathways leading to either alkyl arene. Thus, Curtin–Hammett conditions are likely responsible

for product selectivity, and future catalyst design to target linear products should seek to optimize the thermodynamic bias toward 2,1-insertion and lower the activation barrier for benzene C–H activation from the 2,1-insertion product relative to the 1,2-insertion product. Although the magnitude of the changes in branched/linear selectivity is modest for the current set of catalysts, the results suggest that more dramatic changes in ligand donor ability might have more pronounced changes in selectivity.

## EXPERIMENTAL SECTION

**General Methods.** Unless otherwise noted, all synthetic procedures were performed under anaerobic conditions in a nitrogen filled glovebox or by using standard Schlenk techniques. Glovebox purity was maintained by periodic nitrogen purges and was monitored by an oxygen analyzer ( $O_2 < 15$  ppm for all reactions). Diethyl ether was dried by distillation over  $CaH_2$ . Tetrahydrofuran and *n*-pentane were distilled over sodium/benzophenone and  $P_2O_5$ , respectively. Methylene chloride and benzene were purified by passage through a column of activated alumina. Acetone- $d_6$  and  $CD_2Cl_2$  were used as received and stored under a  $N_2$  atmosphere over 4 Å molecular sieves.  $^1H$  NMR spectra were recorded on a Varian Mercury 300 or Unity Innova 500 MHz or on a Bruker 800 MHz spectrometer.  $^{13}C$  NMR spectra were recorded using a Varian Mercury 300, Unity Innova 500 MHz (operating frequency 75 or 125 MHz, respectively) or using a Bruker 800 MHz spectrometer (operating frequency 201 MHz). All  $^1H$  and  $^{13}C$  NMR spectra are referenced against residual proton signals ( $^1H$  NMR) or the  $^{13}C$  resonances ( $^{13}C$  NMR) of the deuterated solvents.  $^{19}F$  NMR (282 MHz operating frequency) spectra were obtained on a Varian 300 MHz spectrometer and referenced against an external standard of hexafluorobenzene ( $\delta = -164.9$  ppm). GC/MS was performed using a Shimadzu GCMS-QP2010 Plus system with a 30 m  $\times$  0.25 mm SHRXISMS column with 0.25 mm film thickness using electron impact (EI) ionization or negative chemical ionization (NCI), which also allows for simulated electron impact (SEI) ionization. Ethylene (99.5%) and propylene (99.5%) were purchased in a gas cylinder from GTS-Welco and used as received. All other reagents were used as purchased from commercial sources. The preparation, isolation, and characterization of 3-phenylcyclohexanone<sup>23</sup> and  $[(N \sim N)Pt(Ph)(THF)][BAR'_4]^{7h,s}$  (**1a–1f** and **2**) have been previously reported.

**Catalytic Olefin Hydrophenylation with Propylene.** A representative catalytic reaction is described.  $[(^t\text{bpy})Pt(Ph)(THF)][BAR'_4]$  (**1b**) (0.019 g, 0.013 mmol) was dissolved in 12.0 mL of benzene containing 0.01 mol % hexamethylbenzene (HMB) relative to benzene as an internal standard. The reaction mixture was placed in a stainless steel pressure reactor, charged with propylene (0.1 MPa), pressurized to a total of 0.8 MPa with  $N_2$ , and heated to 100 °C. After a given time period, the reaction mixture was allowed to cool to room temperature and was analyzed by GC/MS. Peak areas of the products and the internal standard were used to calculate product yields. Cumene production was quantified using linear regression analysis of gas chromatograms of standard samples. A set of five known standards consisting of 2:1, 4:1, 6:1, 8:1, and 10:1 molar ratios of cumene to HMB in benzene were prepared. A plot of the peak area ratios vs molar ratios gave a regression line. For the GC/MS system, the slope and correlation coefficients ( $R^2$ ) for cumene were 0.89 and 0.99, respectively. Identical

procedures were used to quantify the production of *n*-propylbenzene (1.19; 0.99).

**Catalytic Olefin Hydrophenylation with Non-Gaseous Olefinic Substrates.** A representative catalytic reaction is described.  $[(^t\text{bpy})Pt(Ph)(THF)][BAR'_4]$  (**1b**) (0.005 g, 0.003 mmol) was dissolved in 3.0 mL of benzene containing 1-pentene (55  $\mu\text{L}$ , 150 equiv relative to Pt) and 0.01 mol % hexamethylbenzene relative to benzene as an internal standard. The reaction mixture was placed in a glass pressure tube and heated to 100 °C. After a given time period, the reaction mixture was allowed to cool to room temperature and analyzed by GC/MS. Peak areas of the products and the internal standard were used to calculate product yields from linear regression analysis of standard samples. A set of five known standards consisting of 2:1, 4:1, 6:1, 8:1, and 10:1 molar ratios of alkylbenzene to HMB in  $CH_2Cl_2$  were prepared. A plot of the peak area ratios vs molar ratios gave a regression line. For the GC/MS system, the slope and correlation coefficient ( $R^2$ ) for each alkylbenzene is as follows: *n*-pentylbenzene (1.10; 0.99), 2-phenylpentane (1.33; 0.99), phenylcyclohexane (0.33; 0.99), 3-phenylcyclohexanone (0.33; 0.99), 4-phenylbutan-2-one (0.31; 0.99), methyl cinnamate (0.50; 0.99), and methyl 3-phenylpropanoate (0.53; 0.99).

## ASSOCIATED CONTENT

### Supporting Information

Full computational study, including reaction coordinates for all catalyst models. This material is available free of charge via the Internet at <http://pubs.acs.org>.

## AUTHOR INFORMATION

### Corresponding Authors

\*E-mail: [tbg7h@virginia.edu](mailto:tbg7h@virginia.edu).

\*E-mail: [t@unt.edu](mailto:t@unt.edu)

### Notes

The authors declare no competing financial interest.

## ACKNOWLEDGMENTS

T.B.G. and T.R.C. acknowledge The Office of Basic Energy Sciences, U.S. Department of Energy for support of this work (DE-SC0000776 and DE-FG02-03ER15387, respectively).

## REFERENCES

- (1) (a) Foley, N. A.; Lee, J. P.; Ke, Z.; Gunnoe, T. B.; Cundari, T. R. *Acc. Chem. Res.* **2009**, *42*, 585–597. (b) Andreatta, J. R.; McKeown, B. A.; Gunnoe, T. B. *J. Organomet. Chem.* **2011**, *696*, 305–315. (c) Bhalla, G.; Bischof, S. M.; Ganesh, S. K.; Liu, X. Y.; Jones, C. J.; Borzenko, A.; Tenn, W. J., III; Ess, D. H.; Hashiguchi, B. G.; Lokare, K. S.; Leung, C. H.; Oxgaard, J.; Goddard, W. A., III; Periana, R. A. *Green Chem.* **2011**, *13*, 69–81.
- (2) (a) Price, C. C. *Chem. Rev.* **1941**, *29*, 37–67. (b) *Friedel–Crafts and Related Reactions*; John Wiley and Sons: New York, 1964; Vol. 2. (c) Roberts, R. M.; Khalaf, A. A. *Friedel–Crafts Alkylation Chemistry: A Century of Discovery*; Marcel Dekker, Inc.: New York, 1984.
- (3) (a) Lail, M.; Bell, C. M.; Conner, D.; Cundari, T. R.; Gunnoe, T. B.; Petersen, J. L. *Organometallics* **2004**, *23*, 5007–5020. (b) Matsu-moto, T.; Taube, D. J.; Periana, R. A.; Taube, H.; Yoshida, H. *J. Am. Chem. Soc.* **2000**, *122*, 7414–7415.
- (4) Luedtke, A. T.; Goldberg, K. I. *Angew. Chem., Int. Ed.* **2008**, *47*, 7694–7696.
- (5) McKeown, B. A.; Foley, N. A.; Lee, J. P.; Gunnoe, T. B. *Organometallics* **2008**, *27*, 4031–4033.
- (6) (a) De Felice, V.; De Renzi, A.; Tesauro, D.; Vitagliano, A. *Organometallics* **1992**, *11*, 3669–3676. (b) De Felice, V.; Cuccioliato,

M. E.; De Renzi, A.; Ruffo, F.; Tesauro, D. *J. Organomet. Chem.* **1995**, 493, 1–11. (c) Cucciolito, M. E.; De Renzi, A.; Orabona, I.; Ruffo, F.; Tesauro, D. *J. Chem. Soc., Dalton Trans.* **1998**, 1675–1678.

(7) (a) Matsumoto, T.; Periana, R. A.; Taube, D. J.; Yoshida, H. *J. Mol. Catal. A: Chem.* **2002**, 180, 1–18. (b) Oxgaard, J.; Muller, R. P.; Goddard, W. A., III; Periana, R. A. *J. Am. Chem. Soc.* **2004**, 126, 352–363. (c) Oxgaard, J.; Periana, R. A.; Goddard, W. A., III *J. Am. Chem. Soc.* **2004**, 126, 11658–11665. (d) Lail, M.; Arrowood, B. N.; Gunnoe, T. B. *J. Am. Chem. Soc.* **2003**, 125, 7506–7507. (e) Goj, L. A.; Gunnoe, T. B. *Curr. Org. Chem.* **2005**, 9, 671–685. (f) Foley, N. A.; Lail, M.; Lee, J. P.; Gunnoe, T. B.; Cundari, T. R.; Petersen, J. L. *J. Am. Chem. Soc.* **2007**, 129, 6765–6781. (g) Joslin, E. E.; McMullin, C. L.; Gunnoe, T. B.; Cundari, T. R.; Sabat, M.; Myers, W. H. *Organometallics* **2012**, 31, 6851–6860. (h) McKeown, B. A.; Gonzalez, H. E.; Friedfeld, M. R.; Gunnoe, T. B.; Cundari, T. R.; Sabat, M. *J. Am. Chem. Soc.* **2011**, 133, 19131–19152.

(8) (a) McKeown, B. A.; Gonzalez, H. E.; Gunnoe, T. B.; Cundari, T. R.; Sabat, M. *ACS Catal.* **2013**, 3, 1165–1171. (b) McKeown, B. A.; Gonzalez, H. E.; Friedfeld, M. R.; Brosnahan, A. M.; Gunnoe, T. B.; Cundari, T. R.; Sabat, M. *Organometallics* **2013**, 32, 2857–2865.

(9) McKeown, B. A.; Gonzalez, H. E.; Michaelos, T.; Gunnoe, T. B.; Cundari, T. R.; Crabtree, R. H.; Sabat, M. *Organometallics* **2013**, 32, 3903–3913.

(10) Scarso, A.; Colladon, M.; Sgarbossa, P.; Santo, C.; Michelin, R. A.; Strukul, G. *Organometallics* **2010**, 29, 1487–1497.

(11) Liu, Y.; Mao, D.; Xu, D.; Xu, Z.; Zhang, Y. *Synth. Commun.* **2007**, 37, 4389–4397.

(12) Suzuki, Y.; Yasumoto, T.; Mashima, K.; Okuda, J. *J. Am. Chem. Soc.* **2006**, 128, 13017–13025.

(13) Tomasik, P.; Ratajewicz, Z. *Pyridine-Metal Complexes*; John Wiley & Sons, Inc.: New York, 1985; Vol. 14.

(14) Frisch, M. J.; Trucks, G. W.; Schlegel, H. B.; Scuseria, G. E.; Robb, M. A.; Cheeseman, J. R.; Zakrzewski, V. G.; Montgomery, J. A., Jr.; Stratmann, R. E.; Burant, J. C.; Dapprich, S.; Millam, J. M.; Daniels, A. D.; Kudin, K. N.; Strain, M. C.; Farkas, O.; Tomasi, J.; Barone, V.; Cossi, M.; Cammi, R.; Mennucci, B.; Pomelli, C.; Adamo, C.; Clifford, S.; Ochterski, J.; Petersson, G. A.; Ayala, P. Y.; Cui, Q.; Morokuma, K.; Malick, D. K.; Rabuck, A. D.; Raghavachari, K.; Foresman, J. B.; Cioslowski, J.; Ortiz, J. V.; Baboul, A. G.; Stefanov, B. B.; Liu, G.; Liashenko, A.; Piskorz, P.; Komaromi, I.; Gomperts, R.; Martin, R. L.; Fox, D. J.; Keith, T.; Al-Laham, M. A.; Peng, C. Y.; Nanayakkara, A.; Challacombe, M.; Gill, P. M. W.; Johnson, B.; Chen, W.; Wong, M. W.; Andres, J. L.; Gonzalez, C.; Head-Gordon, M.; Replogle, E. S.; Pople, J. A. *Gaussian 03, Revision C.02*; Gaussian, Inc.: Wallingford, CT, 2004.

(15) (a) Becke, A. D. *Phys. Rev.* **1988**, A38, 3098–3100. (b) Lee, C.; Yang, W.; Parr, R. G. *Phys. Rev., B* **1988**, 37, 785–789.

(16) Stevens, W. J.; Basch, H.; Krauss, M. *J. Chem. Phys.* **1984**, 81, 6026–6033.

(17) Grimme, S.; Antony, J.; Ehrlich, S.; Krieg, H. *J. Chem. Phys.* **2010**, 132, 154104/1-19.

(18) (a) Becke, A. D.; Johnson, E. R. *J. Chem. Phys.* **2005**, 122, 154101/1-5. (b) Johnson, E. R.; Becke, A. D. *J. Chem. Phys.* **2005**, 123, 24101/1-7. (c) Johnson, E. R.; Becke, A. D. *J. Chem. Phys.* **2006**, 124, 174104/1-9.

(19) Barone, V.; Cossi, M. *J. Phys. Chem. A* **1998**, 102, 1995–2001.

(20) Hratchian, H. P. *J. Chem. Theory Comput.* **2005**, 1, 61–69.

(21) Kohn, W.; Sham, L. J. *Phys. Rev.* **1980**, A140, 1133–1138.

(22) (a) Shiotsuki, M.; White, P. S.; Brookhart, M.; Templeton, J. L. *J. Am. Chem. Soc.* **2007**, 129, 4058–4067. (b) Fusto, M.; Giordano, F.; Orabona, I.; Ruffo, F.; Panunzi, A. *Organometallics* **1997**, 16, 5981–5987. (c) Friedrich, A.; Ghosh, R.; Kolb, R.; Herdtweck, E.; Schneider, S. *Organometallics* **2009**, 28, 708–718. (d) Bühl, M.; Håkansson, M.; Mahmoudkhani, A. H.; Öhrström, L. *Organometallics* **2000**, 19, 5589–5596.

(23) Hayashi, T.; Sasaki, K. *Chem. Lett.* **2008**, 37, 842–843.